© 2014. Published by The Company of Biologists Ltd | Journal of Cell Science (2014) 127, 3699–3710 doi:10.1242/jcs.147504

RESEARCH ARTICLE

Anillin interacts with microtubules and is part of the astral pathway that defines cortical domains

Chloe van Oostende Triplet*, Melina Jaramillo Garcia*, Husni Haji Bik, Daniel Beaudet and Alisa Piekny‡

ABSTRACT

Cytokinesis occurs by the ingression of an actomyosin ring that separates the cell into two daughter cells. The mitotic spindle, comprising astral and central spindle microtubules, couples contractile ring ingression with DNA segregation. Cues from the central spindle activate RhoA, the upstream regulator of the contractile ring. However, additional cues from the astral microtubules also reinforce the localization of active RhoA. Using human cells, we show that astral and central spindle microtubules independently control the localization of contractile proteins during cytokinesis. Astral microtubules restrict the accumulation and localization of contractile proteins during mitosis, whereas the central spindle forms a discrete ring by directing RhoA activation in the equatorial plane. Anillin stabilizes the contractile ring during cytokinesis. We show that human anillin interacts with astral microtubules and that this interaction is competed by the cortical recruitment of anillin by active RhoA. Anillin restricts the localization of myosin to the equatorial cortex and that of NuMA (part of the microtubule-tethering complex that regulates spindle position) to the polar cortex. The sequestration of anillin by astral microtubules might alter the organization of cortical proteins to polarize cells for cytokinesis.

KEY WORDS: Cytokinesis, Cytoskeleton, Polarity

INTRODUCTION

Cytokinesis occurs by the RhoA-dependent formation and ingression of an actin–myosin ring that cleaves a cell into two daughter cells. Cues from the mitotic spindle ensure that the contractile ring always forms in a position that bisects the spindle to coordinate the division plane with the segregation of sister chromatids (Green et al., 2012; Piekny et al., 2005). When the mitotic spindle is moved to a new location during anaphase, RhoA–GTP accumulates at the new location (Bement et al., 2005), suggesting that the spindle modulates upstream signals for contractile ring assembly. Anillin is a structural component of the ring that scaffolds actin and myosin, and is recruited by active RhoA (Piekny and Maddox, 2010). Anillin also stabilizes RhoA localization, suggesting that there is feedback between downstream components of the contractile ring and RhoA (Piekny and Glotzer, 2008; Zhao and Fang, 2005a). In support of this, anillin interacts with RacGAP50C (also known as Tum, a *Drosophila* homolog of Cyk-4, which is also known as MgcRacGAP or RACGAP1; D'Avino et al., 2008; Gregory et al., 2008) and Ect2 (Frenette et al., 2012); proteins that localize to the central spindle and are required for RhoA activation.

During anaphase, centrosome separation leads to the enrichment of centrosomally derived astral microtubules at the poles, and a lower density of these microtubules in the central plane (Glotzer, 2009). Polar astral microtubules inhibit the accumulation of contractile proteins at the polar cortex. Decreasing polymerized microtubules causes an increase in the breadth of RhoA localization, and more severe microtubule disruption leads to uncontrolled RhoA activity (Bement et al., 2005; Murthy and Wadsworth, 2008). However, part of this increase in active RhoA could be due to the release of GEFH1 (also known as ARHGEF2), a microtubule-associated guanine nucleotide exchange factor (GEF) for RhoA (Chang et al., 2008; Krendel et al., 2002). In early *Caenorhabditis elegans* embryos, mutations in proteins that cause the spindle to shift towards one pole of the embryo and decrease the proportion of astral microtubules that reach the opposite cortex result in the formation of a second cleavage furrow (Tse et al., 2011; Werner et al., 2007). Furthermore, mutations in proteins that shorten the intercentrosome distance and increase the density of microtubules in the equatorial plane block cytokinesis when combined with mutants or laser treatments that also disrupt the central spindle (Bringmann and Hyman, 2005; Dechant and Glotzer, 2003; Werner et al., 2007). Recent studies in *C. elegans* embryos showed that the astral pathway defines the equatorial plane by inhibiting the cortical recruitment of contractile proteins by polar astral microtubules, whereas the central spindle pathway (described below) is required for transition of the broad contractile ring into a discrete ring (Lewellyn et al., 2010). However, the molecular signals that allow communication between the astral microtubules and the cortex are not known. In both *C. elegans* embryos and human cells, proteins that tether astral microtubules to position the anaphase spindle likely influence the division plane. These protein complexes, which include NuMA, stabilize astral microtubules at the polar cortex through dynein–dynactin (Bringmann et al., 2007; Kiyomitsu and Cheeseman, 2013). Another potential component of the astral pathway in *C. elegans* is anillin (ANI-1), which weakly co-sediments with microtubules *in vitro* (Tse et al., 2011). ANI-1 localizes to astral microtubules that contact the cortex, which might stimulate its removal. Myosin also localizes to cortical astral microtubules, supporting a model where the removal of ANI-1 from the cortex could also promote the removal of myosin, causing a change in the organization of the actin–myosin cytoskeleton at the cortex (Tse et al., 2011).

The central spindle is formed during anaphase from overlapping bundled microtubules between sister chromatids, and provides stimulatory cues for furrowing by recruiting the RhoGEF Ect2 (Glotzer, 2009; Somers and Saint, 2003; Yüce

Department of Biology, Concordia University, Montreal, QC H4B 1R6, Canada.
*These authors contributed equally to this work

‡Author for correspondence (alisa.piekny@concordia.ca)

Received 5 December 2013; Accepted 12 June 2014

Journal of Cell Science (2014) 127, 3699–3710 doi:10.1242/jcs.147504

et al., 2005; Zhao and Fang, 2005b). In metaphase, Ect2 is phosphorylated by Cdk1, which causes it to fold into an inactive conformation (Saito et al., 2003; Yüce et al., 2005). At anaphase onset, this phosphorylation is removed, permitting Ect2 to bind to the centralspindlin protein Cyk-4, which is part of the centralspindlin complex with MKLP1 (also known as KIF23) (Yüce et al., 2005; Zhao and Fang, 2005b). Cyk-4 is also phosphorylated by Plk1 to promote its interaction with Ect2 (Petronczki et al., 2007; Wolfe et al., 2009; Yüce et al., 2005; Zhao and Fang, 2005b). Ect2 likely requires Cyk-4 binding for its activation, because Plk1 inhibition or Cyk-4 depletion phenocopies the loss of Ect2 or RhoA (Petronczki et al., 2007; Wolfe et al., 2009; Yüce et al., 2005; Zhao and Fang, 2005b). Both Cyk-4 and Ect2 have regions that mediate their interaction with the overlying membrane, and might help to regulate their activity *in vivo* (Frenette et al., 2012; Lekomtsev et al., 2012; Su et al., 2011). As long as Ect2–Cyk-4 complexes are permitted to form, central-spindle-labeled microtubules are dispensable for contractile ring formation. In MKLP1-depleted or Aurora-B-inhibited cells, the central spindle is not stably formed, yet contractile ring proteins still accumulate at the equatorial cortex. Their localization is broader in comparison with that of control cells; however, they do not localize to the poles of the cell, and furrows still form and ingress in many of the cells (Yüce et al., 2005). Furthermore, in *C. elegans* embryos, depletion of *spd-1* (a PRC1 homolog that bundles central spindle microtubules) has no effect on contractile ring formation or ingression (Lewellyn et al., 2010; Verbrugghe and White, 2004). Therefore, pathways associated with astral microtubules, or additional non-microtubule-based pathways, regulate the localization of contractile proteins to define cortical domains (Kiyomitsu and Cheeseman, 2013; Sedzinski et al., 2011; von Dassow et al., 2009).

The ability of astral microtubules to inhibit the cortical accumulation of contractile proteins is not restricted to *C. elegans* embryos. In fused Ptk1 cells (a marsupial cell line), furrows form between the two asters where no central spindle is present, although overlapping microtubules could become bundled and recruit Ect2 (Oegema et al., 2000). However, a theoretical minimum density of microtubules likely occurs between the two asters, removing inhibitory signals in this region to permit the recruitment of contractile ring proteins. Furthermore, contractile proteins are recruited in nocodazole-arrested cells treated with a Cdk1 inhibitor, and cells form ectopic furrows (Canman et al., 2000; Petronczki et al., 2007). However, other studies in human cells suggest that astral microtubules can have a stimulatory role in furrowing, particularly if they are stabilized towards the cortex (Canman et al., 2003; Hu et al., 2008; Shannon et al., 2005). Similar to the Ptk1 cells, these microtubules might be bundled by central spindle proteins and recruit Ect2 (Foe and von Dassow, 2008; Hu et al., 2008). Therefore, it is not clear how astral microtubules define the division plane in human cells, particularly because human cells have more prominent central spindles in comparison to those of sea urchin or *C. elegans* embryos.

We show that the division plane in HeLa cells is determined by an astral-dependent mechanism similar to that of *C. elegans* embryos (Lewellyn et al., 2010; Tse et al., 2011). Astral and central spindle microtubules independently determine the localization of contractile proteins during cytokinesis. Previously, we found that although furrows form and ingress in HeLa cells with disrupted central spindles (after MKLP1 depletion), co-depletion of MKLP1 and anillin completely blocked furrowing (Piekny and Glotzer, 2008), suggesting that anillin functions with astral microtubules to define the division plane. In support of this hypothesis, we found that anillin localizes to astral microtubules and becomes further enriched on microtubules after their stabilization by RNA interference (RNAi)-mediated knockdown of MCAK (also known as KIF2C) or taxol treatment. The microtubule localization of anillin is also enriched after C3 treatment or Ect2 depletion, suggesting that active RhoA competes with microtubules for anillin localization. Furthermore, anillin is required for the restricted localization of nonmuscle myosin at the equatorial cortex and for that of NuMA at the polar cortex. Depleting anillin from cells with overextended astral microtubules reduces their ability to restrict cortical proteins, suggesting that anillin might polarize the cortex through astral microtubules.

RESULTS

Astral microtubules and central spindle microtubules independently regulate the localization of contractile proteins

In *C. elegans* embryos, astral microtubules restrict the localization of contractile proteins to the equatorial plane, whereas the central spindle forms a focused contractile ring (Lewellyn et al., 2010). In human cells, studies have shown that astral or central spindle microtubules control the localization of contractile proteins (Murthy and Wadsworth, 2008; Yüce et al., 2005), but it was not shown how they work together to define the division plane. To determine how astral microtubules restrict the localization of contractile proteins in HeLa cells, we lengthened these microtubules by depleting MCAK and looked at changes in the localization of anillin and RhoA (tubulin localization is shown in supplementary material Fig. S1; RNAi efficiency is shown in supplementary material Fig. S2; Rankin and Wordeman, 2010; Zanin et al., 2013). These observations were quantified by measuring anillin fluorescence intensity across the central plane of the cell to include the equatorial cortex (the line scan was drawn away from the DNA in metaphase cells) and averaging cells with identical line lengths. In control metaphase cells, anillin was cytosolic and weakly recruited to microtubules (Fig. 1A). This pattern persisted into early anaphase, although anillin also was weakly recruited to the cortex at this stage (Fig. 1A). By late anaphase, anillin strongly accumulated at the equatorial cortex and remained associated with the cortex during furrow ingression (Fig. 1A). RhoA localization closely matched anillin localization throughout mitosis, except RhoA was not visible on microtubules in metaphase or early anaphase cells (Fig. 1A). The localization of anillin and RhoA in metaphase MCAK-RNAi cells was similar to that of control cells. However, anillin and RhoA were not recruited to the cortex in early anaphase MCAK-depleted cells (Fig. 1A; supplementary material Fig. S1). In late anaphase and ingressing telophase MCAK-depleted cells, anillin and RhoA localized to the equatorial cortex, but their localization appeared to be more restricted in comparison to that of control cells (Fig. 1A; supplementary material Fig. S1). To further quantify the effect of MCAK depletion on anillin localization, the levels of anillin fluorescence at the equatorial cortex were measured as a ratio of total anillin (Fig. 1B). These data showed that levels of anillin were significantly lower at the equatorial cortex after MCAK depletion in comparison to those of control cells (Fig. 1B). In addition, we measured the ratio of the breadth of anillin localization to cell length, and found that anillin was

Journal of Cell Science (2014) 127, 3699–3710 doi:10.1242/jcs.147504

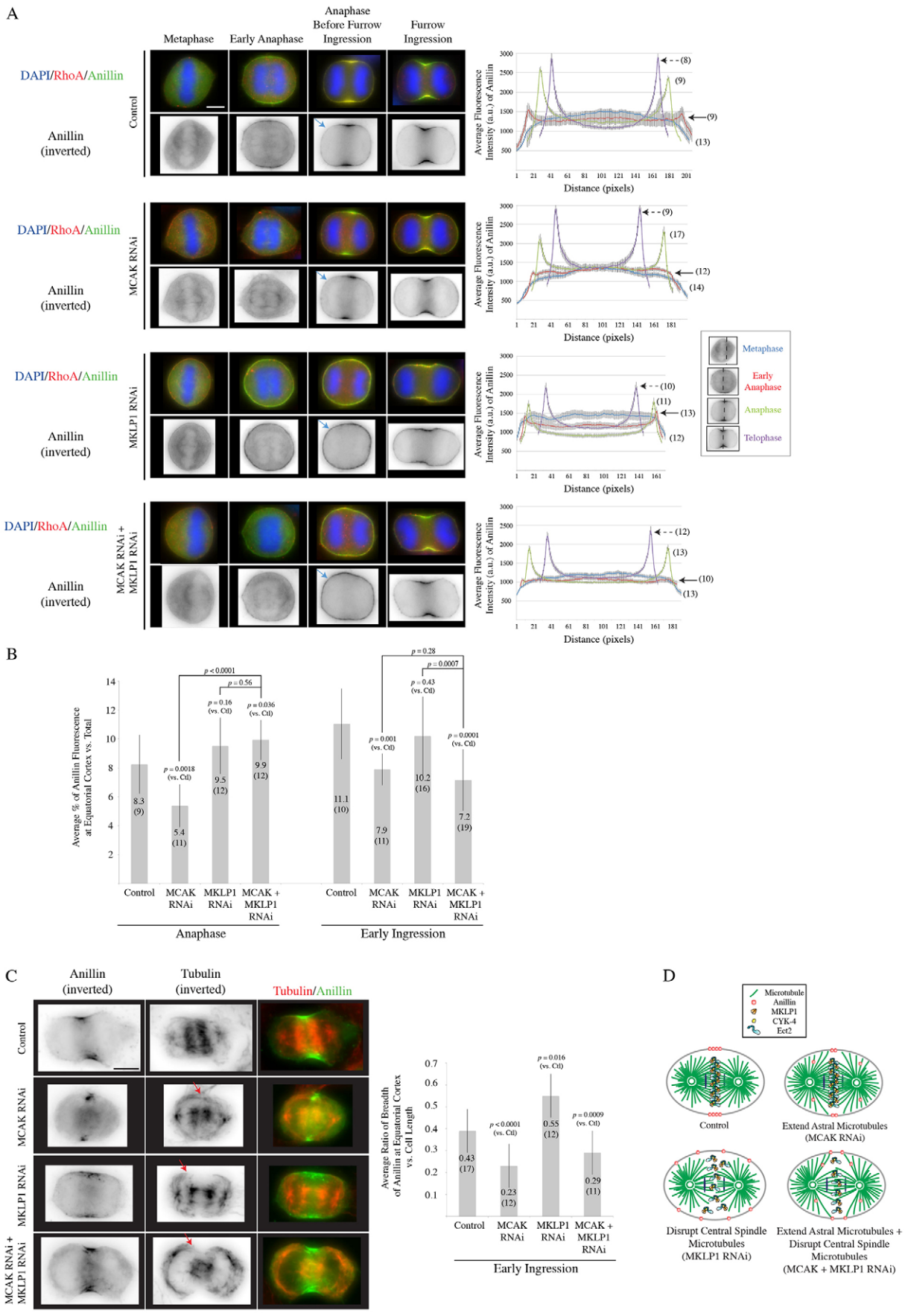

Fig. 1. See next page for legend.

Journal of Cell Science (2014) 127, 3699–3710 doi:10.1242/jcs.147504

Fig. 1. Astral and central spindle microtubules restrict the localization of contractile ring proteins. (A) Left, fixed HeLa cells at various stages of mitosis treated with MCAK RNAi, MKLP1 RNAi or both stained for RhoA, anillin and DNA (DAPI). Blue arrows, polar cortex. Right, graphs show the average fluorescence intensity of anillin (a.u., arbitrary units) across the equatorial plane (distance in pixels) at the indicated stages. The data show the mean±s.e.m.; *n* values are shown in brackets. (B) Graph shows the average anillin fluorescence at the equatorial cortex versus total signal. Ctl, control. (C) Left, *Z*-stack projections of fixed HeLa cells stained for anillin, tubulin and DNA (DAPI) after MCAK RNAi, MKLP1 RNAi or co-depletion. Red arrows, the boundaries of astral microtubules. Scale bars: 10 μm. Right, a bar graph showing the average ratio of breadth of anillin at the equatorial cortex to cell length in early ingressing cells. For B and C, data show the mean±s.d.; *P*-values were calculated by using Student's *t*-tests; *n* values are shown in brackets below each mean. (D) Schematic to show how various treatments alter the breadth and intensity of anillin localization at the equatorial cortex.

significantly more restricted in MCAK-depleted cells in comparison to control cells (Fig. 1C). Taken together, our data show that overextending microtubules delays the cortical recruitment of anillin and RhoA in early anaphase, and continues to restrict their localization during ingression (Fig. 1).

Next, we selectively disrupted astral microtubules to further demonstrate their ability to restrict contractile proteins. We expanded on previous studies by also including metaphase and early anaphase cells (Fig. 2A; Murthy and Wadsworth, 2008). The concentration of nocodazole (30 ng/ml) used for this experiment preferentially removed polar astral microtubules but left some of the central spindle microtubules intact (supplementary material Fig. S3A; Zanin et al., 2013). Anillin fluorescence was measured across the central plane of cells at various mitotic stages (Fig. 2A). Anillin and RhoA localized more strongly to the cortex in nocodazole-treated metaphase and early anaphase cells in comparison to control cells (Fig. 2A). Anillin was also enriched in anaphase cells and in ingressing cells, and the breadth of anillin and RhoA enrichment was increased along the equatorial cortex in comparison to that of control cells. The change in anillin localization was quantified by measuring the ratio of anillin at the equatorial cortex to total anillin. Indeed, levels of cortical anillin were significantly higher in anaphase and ingressing nocodazole-treated cells in comparison to those of control cells (Fig. 2A). These data support a model where astral microtubules restrict the cortical localization of anillin and RhoA in mitotic cells.

Next, we determined how the central spindle contributes to the localization of contractile proteins. We depleted MKLP1 to disrupt the central spindle, and we monitored the localization of anillin and RhoA (Mishima et al., 2002). Several complexes localize to the central spindle, including the chromosomal passenger complex (CPC), which comprises Aurora B, INCENP and Survivin (also known as BIRC5) (Carmena et al., 2012). Their localization is partly altered in MKLP1-depleted cells and was used to verify central spindle disruption (supplementary material Figs S1, S2). In MKLP1-depleted metaphase and early anaphase cells, anillin and RhoA localization resembled that of control cells (Fig. 1A). However, in MKLP1-depleted anaphase cells, anillin and RhoA spread around the entire cortex, unlike control cells where anillin and RhoA were restricted to the equatorial plane (Fig. 1A). In ingressing MKLP1-depleted telophase cells, anillin and RhoA cleared from the poles of the cell, but were more broadly localized in comparison to their localization in control cells (Fig. 1A,C). In anaphase and ingressing MKLP1-depleted cells, the peak intensity of anillin was lower in comparison to that of control cells, yet the amount of anillin at the equatorial cortex was not significantly different based on the ratio of accumulated anillin to total anillin (Fig. 1B). Our data show that the central spindle promotes the accumulation of RhoA in a discrete region and, in telophase, helps to form a tight contractile ring, similar to that observed in *C. elegans* embryos (Lewellyn et al., 2010).

We then determined how astral microtubules and the central spindle work together to regulate the localization of contractile proteins by examining their localization after co-depletion of MCAK (to overextend astral microtubules) and MKLP1 (to disrupt the central spindle; supplementary material Figs S1, S2). Co-depleted metaphase cells resembled control cells, with little change in anillin or RhoA localization (Fig. 1A), whereas early anaphase cells showed the MCAK RNAi phenotype, with no cortical RhoA or anillin localization (Fig. 1A). Interestingly, anillin and RhoA localized around the entire cortex in co-depleted anaphase cells, similar to the pattern observed in MKLP1-depleted cells (Fig. 1A). However, in co-depleted telophase cells, anillin and RhoA were more restricted in comparison to control cells (Fig. 1A,C). In addition, the peak intensity of anillin fluorescence in co-depleted cells remained lower in comparison to that of control cells (Fig. 1A,B). In anaphase, the ratio of anillin at the equatorial cortex versus total anillin was not significantly different between the co-depleted cells and MKLP1-RNAi or control cells (Fig. 1B). However, in telophase, the ratio of anillin at the equatorial cortex was significantly lower in the co-depleted cells in comparison to control cells (Fig. 1B). These data suggest that astral microtubules and the central spindle function independently to polarize the cortex (Fig. 1D). In early anaphase and telophase, astral microtubules restrict the localization of contractile proteins, whereas the central spindle helps to form a tight contractile ring during late anaphase and telophase.

To further study how the central spindle and astral microtubules work together, astral microtubules were removed from cells with disrupted central spindles. Depolymerization of astral microtubules using a low dose of nocodazole, or disruption of the central spindle using MKLP1 RNAi, caused contractile proteins to spread along the equatorial cortex in ingressing cells, but anillin did not localize to the polar cortex (Fig. 1A; Fig. 2A; supplementary material Fig. S3B). Depolymerization of astral microtubules in MKLP1-depleted cells caused anillin to localize around the entire cortex in 45.5% of the cells ($n=11$; supplementary material Fig. S3B). These data suggest that both sets of microtubules independently contribute to the localization of contractile proteins. Alternative mechanisms, including chromatin-based and MP-GAP (also known as ARHGAP11A), likely restrict anillin localization in the absence of microtubules (Kiyomitsu and Cheeseman, 2013; Zanin et al., 2013).

The boundary of accumulated anillin correlates with astral microtubules near the equatorial cortex

In HeLa cells, the division plane is determined by astral and central spindle microtubules. Whereas the central spindle recruits the GEF Ect2 to activate RhoA, the only known components of the astral pathway regulate spindle positioning (Bringmann et al., 2007; Kiyomitsu and Cheeseman, 2013). Recent studies in *C. elegans* embryos suggest that ANI-1, anillin, could be a component of the astral pathway (Tse et al., 2011). ANI-1 directly interacts with microtubules, which could promote its removal from the cortex and

Journal of Cell Science (2014) 127, 3699–3710 doi:10.1242/jcs.147504

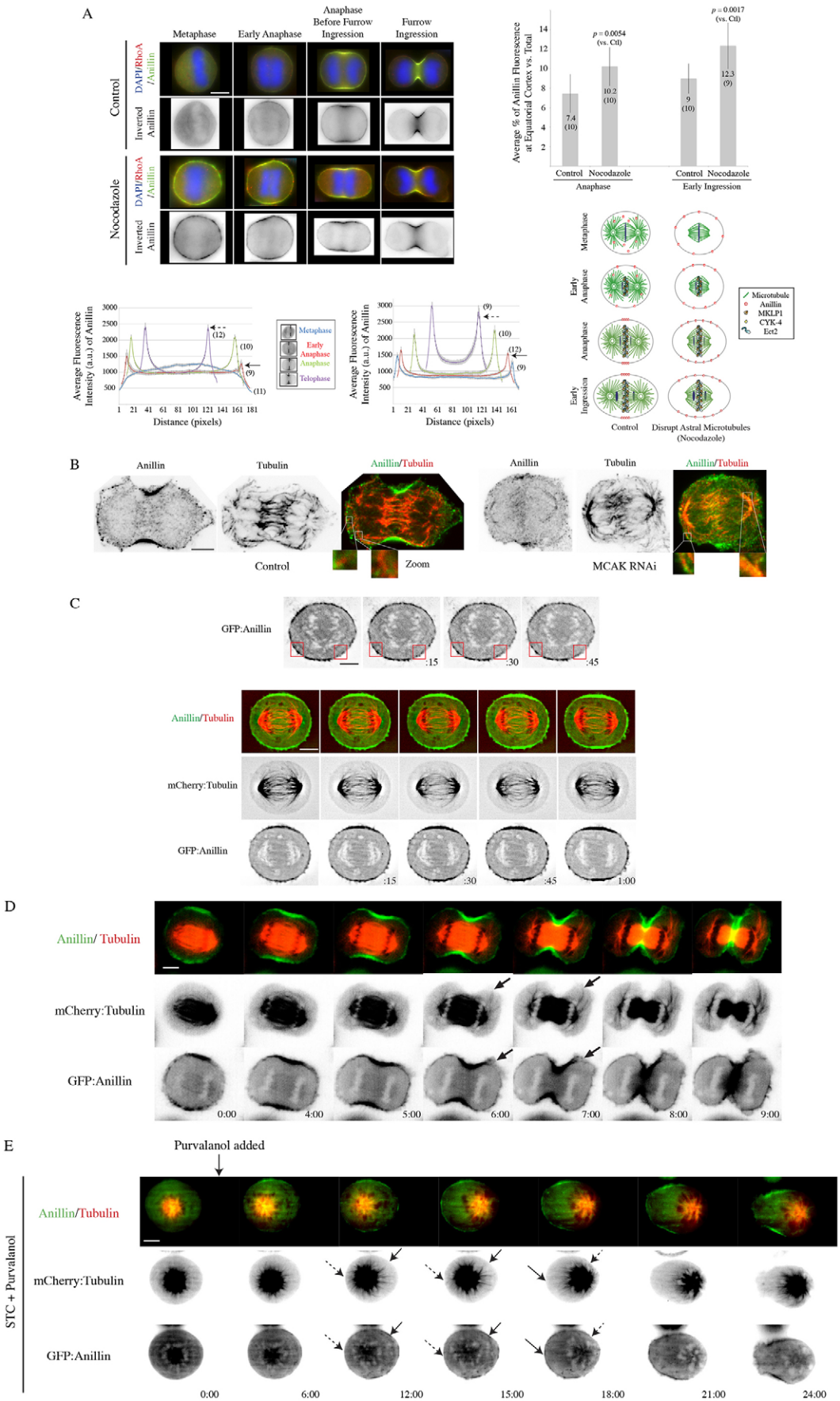

Fig. 2. See next page for legend.

Journal of Cell Science (2014) 127, 3699–3710 doi:10.1242/jcs.147504

Fig. 2. Astral microtubules regulate the localization of contractile proteins. (A) Upper left, fixed HeLa cells treated with nocodazole (30 ng/ml) for 10 minutes were stained for anillin, RhoA and DNA (DAPI). Lower left, graphs show the average intensity of anillin (a.u., arbitrary units) across the equatorial plane (distance in pixels) of cells at the indicated stages. Data show the mean±s.e.m.; *n* values are shown in brackets. Upper right, graph shows the proportion of anillin at the equatorial cortex as indicated. Data show the mean±s.d.; *P*-values were calculated by using Student's *t*-test; *n* values are shown in brackets below each mean. Lower right, schematic shows the impact of nocodazole treatment on the localization of anillin in early mitosis. (B) Confocal images of a control or MCAK-depleted HeLa cell stained for anillin and tubulin are shown. Boxes indicate magnified regions (~4×) to show anillin and microtubules. (C) Upper panel, single-plane images of a live cell stably expressing GFP–anillin filmed at 15-second intervals. The red boxes highlight regions of the cortex. Lower panel, *Z*-stack projections of central planes from a live cell coexpressing GFP–anillin (spectrally unmixed) and mCherry–tubulin at 15-second intervals during anaphase. (D) *Z*-stack projections of central planes from a live HeLa cell coexpressing GFP–anillin (spectrally unmixed) and mCherry–tubulin filmed through cytokinesis. Arrows, astral microtubules near the cortex where anillin clears. (E) Central planes from a cell coexpressing GFP–anillin (spectrally unmixed) and mCherry–tubulin treated with STC and purvalanol. The times after addition of purvalanol are shown. Dashed arrows, astral microtubules and clearing of cortical anillin; solid arrows, regions where anillin is more cortical. Scale bars: 10 μm.

alter the organization of contractile proteins. Astral microtubules restrict the localization of anillin in HeLa cells, and the zone of accumulated anillin appears to match the boundaries of astral microtubules (Fig. 1). To examine this more closely, we performed confocal microscopy on cells immunostained for anillin and tubulin, and compared control cells to cells depleted of MCAK (Fig. 2B). In both cell types there were dots of anillin decorating the astral microtubules (Fig. 2B).

We also visualized the localization of anillin and microtubules in live cells during cytokinesis. Similar to anillin in fixed early anaphase cells, GFP–anillin weakly localized to microtubules and at the cortex (Fig. 2C). Stripe-like patterns of anillin were visible throughout the cell, some of which extended from the cortex (Fig. 2C). Strikingly, when mCherry-labeled microtubules approached the cortex adjacent to the equatorial region, GFP–anillin cleared from this region and blebbing was observed (6/10 cells; Fig. 2C,D). GFP–anillin and mCherry–tubulin were also imaged in live cells induced to be monopolar (Fig. 2E). S-trityl cysteine (STC) prevents centrosome separation, causing cells to arrest in prometaphase, and Cdk1 inhibition promotes cell cycle exit (Hu et al., 2008). As the cells exit, they polarize, with 'central-spindle-labeled' microtubules pointing towards the polarizing cortex and 'astral' microtubules emanating towards the opposite pole (Hu et al., 2008). GFP–anillin was cytosolic and observed on microtubules in STC-treated cells and was recruited to the cortex after Cdk1 inhibition with purvalanol (Fig. 2E). As the astral portion of the monopolar spindle neared the cortex, anillin was cleared from this region and subsequently accumulated on the opposite polarizing cortex (Fig. 2E). Therefore, the cortical localization of anillin responds to the position of astral microtubules *in vivo*.

Anillin localizes to astral microtubules and binds to microtubules *in vitro*

Previous studies have shown that the astral pathway functions redundantly with the central spindle pathway to determine the division plane in *C. elegans* embryos (Bringmann and Hyman, 2005; Dechant and Glotzer, 2003; Werner et al., 2007). Although disruption of either pathway does not disrupt furrowing, disrupting both pathways blocks furrowing altogether (Bringmann et al., 2007; Werner et al., 2007). We previously showed that co-depletion of anillin and MKLP1 blocks furrow ingression in HeLa cells (Piekny and Glotzer, 2008). We extended this experiment by observing the localization of GFP–MLC (nonmuscle myosin light chain; active; T18E S19E) in anillin-RNAi, MKLP1-RNAi or co-depleted cells (supplementary material Fig. S2; Fig. S4A). As expected, furrowing was blocked and active myosin localized around the entire cortex after co-depletion of anillin and MKLP1 (supplementary material Fig. S4A).

In *C. elegans* embryos, ANI-1 colocalizes with astral microtubules and co-sediments with microtubules *in vitro* (Tse et al., 2011). To determine whether human anillin also associates with microtubules, we analyzed changes in anillin localization after taxol treatment, by measuring the ratio of anillin at the equatorial cortex versus that inside the cell within the vicinity of microtubules. After only 5 minutes of 10 μM taxol treatment, the localization of anillin to microtubules significantly increased at the expense of its cortical localization, and anillin was almost fully redistributed to microtubules after 20 minutes (Fig. 3A). These data suggest that the affinity of human anillin for microtubules might depend on microtubule stability.

To further characterize the association of anillin with microtubules, we examined changes in the localization of anillin after MCAK depletion. Our earlier data showed that anillin is enriched in the cytosol and on microtubules after MCAK depletion (Fig. 1; Fig. 2B). Consistent with these data, anillin partially overlapped with EB1–2EGFP at the plus ends of microtubules in MCAK-depleted early anaphase cells (Fig. 3B). To quantify the localization of anillin on microtubules, we measured the average intensity of anillin along the equatorial (cortex and cytosol) and longitudinal planes (cytosol and microtubules) in early anaphase and anaphase cells (supplementary material Fig. S4B). In early anaphase, the levels of cortical anillin decreased, with a concomitant increase in anillin in the cytosol and on spindle microtubules. In MCAK-depleted anaphase cells, although anillin was still recruited to the cortex, cytosolic pools remained slightly higher in comparison to those of control cells. Therefore, microtubules could act as a localization sink for anillin.

Our data suggest that the microtubule localization of anillin could be competed by the cortex. Because active RhoA is required for the accumulation of anillin at the equatorial cortex, we decreased the levels of active RhoA and examined changes in anillin localization. In C3-treated (to specifically target RhoA) or Ect2-RNAi cells (to target the GEF for RhoA), anillin accumulated on microtubules, particularly during stages of mitosis when anillin is enriched at the equatorial cortex in control cells (deconvolved images more clearly show the localization of anillin to microtubules; Fig. 3C). This data shows that active RhoA could compete with microtubules for anillin localization, and anillin has a preference for stable microtubules (e.g. those that might reach and remain near the cortex, or are bundled).

Lastly, we determined whether human anillin directly binds to microtubules *in vitro*. Previously, the C-terminus of ANI-1 was shown to weakly co-sediment with microtubules, but the microtubule-binding region was not mapped to a precise location (Tse et al., 2011). Furthermore, it is not known whether all the various protein interactions are conserved between human anillin and ANI-1. We performed co-sedimentation assays using

Journal of Cell Science (2014) 127, 3699–3710 doi:10.1242/jcs.147504

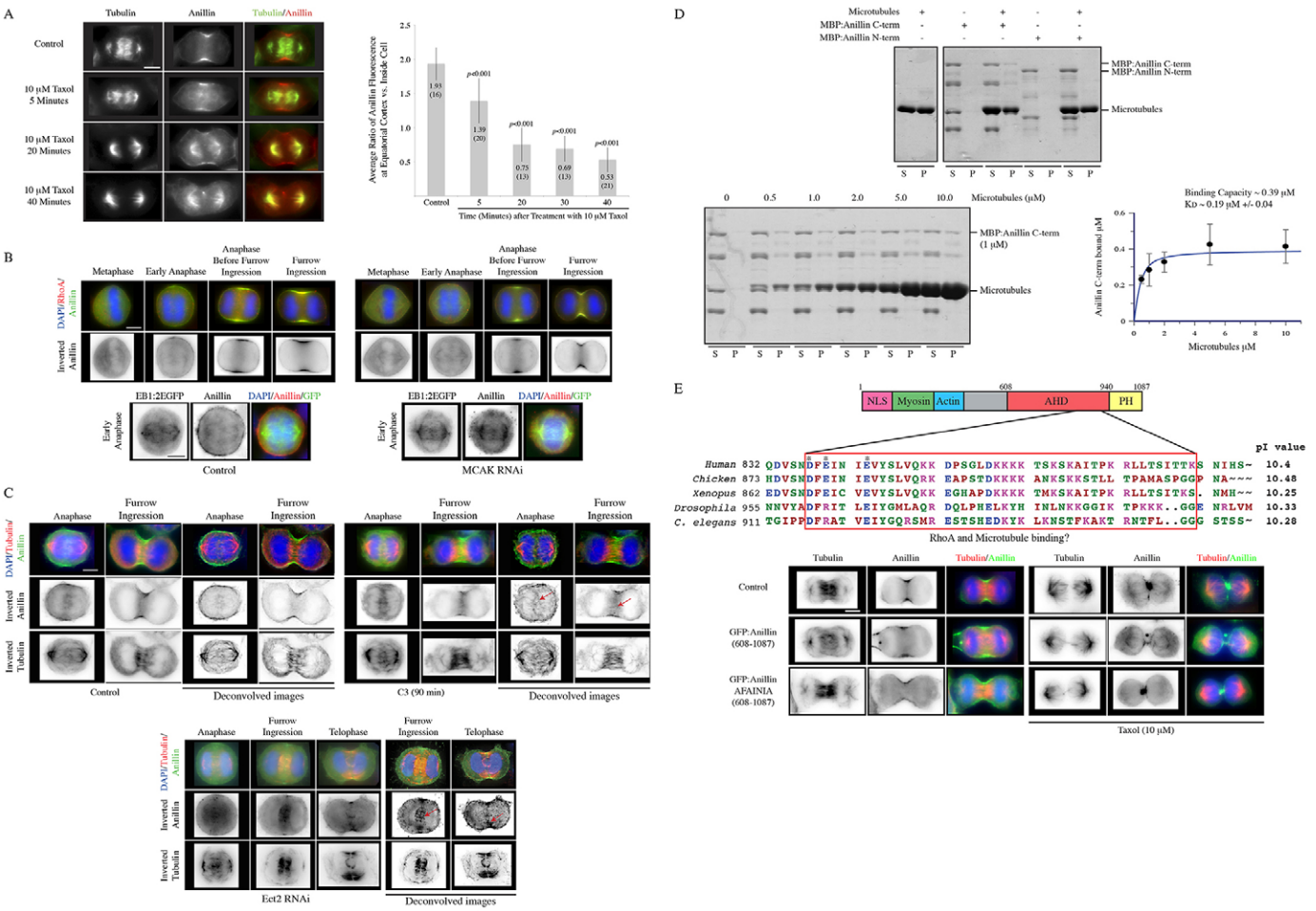

Fig. 3. Anillin interacts with microtubules. (A) Left, fixed HeLa cells treated with 10 μM taxol for the indicated times were stained for tubulin and anillin. Right, graph shows the average ratio of anillin (a.u., arbitrary units) at the equatorial cortex to that at regions near microtubules for the indicated times points. Data show the mean±s.d.; *P*-values were calculated by using Student's *t*-test; *n* values are shown in brackets. (B) Upper panels, fixed mitotic HeLa cells (control or treated with MCAK RNAi) stained for RhoA, anillin and DNA (DAPI). Lower panels, fixed early anaphase cells expressing EB1–2GFP stained for GFP, anillin and DNA. (C) *Z*-stack projections from central planes of fixed control HeLa cells, along those of cells treated with C3 or Ect2 RNAi, stained for tubulin, anillin and DAPI. Deconvolved images are shown as indicated. Red arrows, microtubules. (D) A Coomassie-stained gel of a co-sedimentation assay with 2.5 μM purified microtubules and 1 μM purified MBP-tagged anillin C-terminus (C-term, 608–1087) or N-terminus (N-term, 100–460). S, supernatant; P, pellet. Also shown is a Coomassie-stained gel of a co-sedimentation assay with 1.0 μM of anillin C-terminus and increasing concentrations of microtubules. The graph shows the average amounts of bound anillin C-terminus (μM). Data show the mean±s.d.; $n=3$ assays. (E) Amino acid sequence alignments of anillin homologs from various organisms as indicated (ANI-1 from *C. elegans*; isoform A from *Drosophila*). Amino acids that coordinate RhoA binding are indicated by an asterix. The red box shows the region used to calculate the pI value for each homolog. D and E are in blue; K and R are in pink; G, H, N, T, S, Q are in green; and L, M, F, P, I and V are in red. *Z*-stack projections of central planes of fixed HeLa cells expressing GFP-tagged anillin C-terminus (608–1087) or mutant C-terminus (DFEINIE – AFAINIA) with and without taxol treatment are shown. NLS, nuclear localization sequence; AHD, anillin homology domain; PH, pleckstrin homology. Scale bars: 10 μm.

1 μM of a purified MBP-tagged N-terminal or C-terminal half of human anillin with 2.5 μM of microtubules. As shown in Fig. 3D, the C-terminal half of anillin co-sedimented with microtubules, but the N-terminal half did not. We further characterized the affinity of the C-terminus for microtubules by performing a series of co-sedimentation assays with 1 μM of anillin and increasing concentrations of tubulin (0.5–10 μM). Binding capacity was reached at 0.39 μM, and the resulting curve was consistent with a 1:1 stoichiometry and a mean K_D of 0.19±0.04 μM (±s.d.; Fig. 3D). These results suggest that human anillin also binds directly to microtubules, and there might be a conserved site among anillin homologs in the C-terminus.

Previously characterized microtubule-binding sites in other proteins contain stretches of basic residues (e.g. Solinet et al., 2013). Interestingly, part of the C-terminus of anillin from human, chicken, frog, *Drosophila* and *C. elegans* had isoelectric points (pI) of >10 (Innovagen peptide property calculator) in a region previously shown to enhance RhoA binding (Fig. 3E; Piekny and Glotzer, 2008). To determine whether the same site is required for both interactions, we examined the localization of a GFP-tagged C-terminal fragment of anillin containing the mutations of the sequence DFEINIE to AFAINIA (Fig. 3E). These mutations decrease but do not abolish RhoA binding, and constructs containing these mutations retain cortical localization (Piekny and Glotzer, 2008). Whereas non-mutant anillin localized to taxol-stabilized microtubules similar to endogenous anillin, the mutant failed to localize to microtubules (Fig. 3E). Although these mutations do not decrease the pI, they likely impart

Journal of Cell Science (2014) 127, 3699–3710 doi:10.1242/jcs.147504

structural changes that affect both RhoA and microtubule binding. Therefore, this data suggests that the RhoA and microtubule-binding sites directly overlap.

Anillin polarizes the cortex through astral microtubules

Next, we wanted to determine the relationship between anillin and astral microtubules *in vivo*. If anillin alters the localization of contractile proteins through its association with astral microtubules, then the overextension of astral microtubules (e.g. by MCAK RNAi) should have no effect on their localization after anillin depletion. Consistent with our data on anillin, the zone of accumulated GFP–MLC (active) at the equatorial cortex was more restricted in MCAK-RNAi cells in comparison to control cells (Fig. 4A; supplementary material Fig. S2). Interestingly, we consistently observed two phenotypes in anillin-RNAi cells – one set of cells displayed failed furrow ingression (24%), whereas the second set of cells oscillated as described previously (76%; Fig. 4A; supplementary material Fig. S2). In all of the anillin-depleted cells, GFP–MLC (active) localized broadly or around the entire cortex (Fig. 4A). All cells co-depleted of MCAK and anillin displayed oscillations with myosin moving around the cortex, although the degree of ingression varied from cell to cell (Fig. 4A; supplementary material Fig. S2). To quantify changes in myosin localization, we determined the breadth of accumulated GFP–MLC (active) at the equatorial cortex by measuring the number of pixels with levels of GFP–MLC fluorescence greater than half the maximal value at early ingression (Fig. 4B). The breadth of myosin localization significantly decreased in MCAK-RNAi cells, whereas it increased in anillin-RNAi cells, and was close to the control value in the co-depleted cells. The ratio of the breadth at the equatorial cortex to cell length was similar to the breadth measurements, suggesting that the changes in breadth were not due to changes in cell length (Fig. 4B). Because myosin was no longer restricted by overextended astral microtubules in the co-depleted cells, these results suggest that anillin influences the localization of contractile proteins in response to changes in the astral microtubules. However, myosin clearance from the polar cortex in the co-depleted cells suggests that alternative mechanisms also regulate myosin localization.

We also wanted to determine whether anillin is required for the localization of proteins at the polar cortex. NuMA is a component of the microtubule-tethering complex that positions the mitotic spindle (Kiyomitsu and Cheeseman, 2013). NuMA localizes to the spindle poles and polar cortex as cells progress through anaphase and early telophase, then localizes in the vicinity of chromatin during telophase (Fig. 5A). To quantify changes in NuMA localization, the zone of GFP–NuMA clearance was determined using the number of pixels with levels matching cytosolic values (Fig. 5B). In MCAK-depleted cells, the zone of GFP–NuMA clearance was smaller than in control cells, consistent with the equatorial restriction of myosin (Fig. 5A,B).

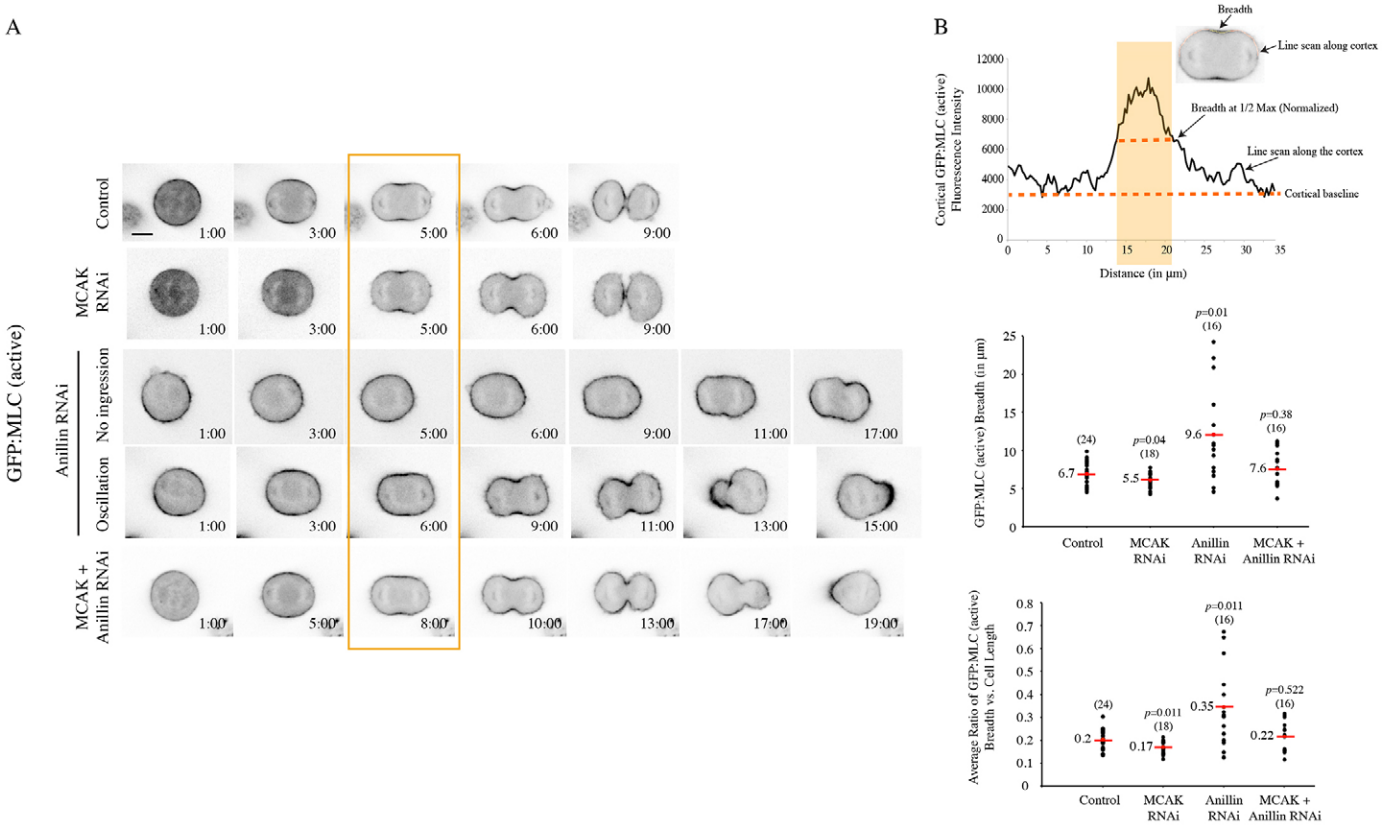

Fig. 4. Anillin regulates the localization of contractile proteins through microtubules. (A) Images of live HeLa cells stably expressing GFP–MLC (active) treated with MCAK RNAi, anillin RNAi or both from the onset of anaphase, along with controls. The orange box highlights the time-point used to measure breadth. Scale bar: 10 µm. (B) Upper panel, the graph shows a cortical line scan, and the pixels that correspond to half maximum levels are highlighted by the shaded orange box (also shown by the top orange dotted line). The cortical baseline is also indicated. Middle panel, the graph shows the breadth (in µm) of enriched GFP–MLC (active) for each treatment. Lower panel, the graph shows the average ratio of GFP–MLC breadth versus cell length. For the middle and lower panels, the red line shows the mean value; *P*-values were calculated by using Student's *t*-test; *n* values are indicated in brackets.

Journal of Cell Science (2014) 127, 3699–3710 doi:10.1242/jcs.147504

In anillin-depleted cells, NuMA localized around the entire cortex in non-ingressing cells, or was cleared from only a small region in oscillating cells (Fig. 5A,B). In MCAK and anillin co-depleted cells, NuMA similarly was rarely cleared from the cortex (Fig. 5A,B). We also examined the localization of GFP-tagged Arp1A (also known as α-centractin), which is part of the dynein–dynactin complex that responds to changes in cortical NuMA (Kiyomitsu and Cheeseman, 2012). In control cells, GFP–Arp1A localized to the polar cortex, similar to NuMA (Fig. 5C). In anillin-depleted cells, GFP–Arp1A was no longer restricted to the polar cortex, consistent with changes in NuMA localization (Fig. 5C). This data suggests that anillin is essential for regulating the localization of proteins at the polar cortex, regardless of changes in astral microtubules.

DISCUSSION

We propose that, similar to *C. elegans* embryos, astral and central spindle microtubules independently define the division plane (Lewellyn et al., 2010). First, astral microtubules prevent the recruitment of contractile proteins in metaphase and early anaphase. During late anaphase, the central spindle promotes the accumulation of contractile proteins in a discrete zone at the equatorial cortex. During telophase, both the central spindle (through the directed activation of RhoA) and astral microtubules (possibly by promoting the removal of anillin) restrict the localization of contractile proteins to form a tight contractile ring. Our data support a role for anillin as a molecular component of the astral pathway that regulates the localization of cortical proteins in response to astral microtubules. Similar to *C. elegans* ANI-1, human anillin localizes to microtubules and can bind to microtubules *in vitro* (Tse et al., 2011). The microtubule-binding site maps to the C-terminus of anillin, and one hypothesis is that the interaction of anillin with RhoA directly competes with its ability to interact with microtubules. Therefore, when levels of active RhoA are low during metaphase and early anaphase, anillin is in the cytosol and on microtubules, but when active RhoA levels are high during anaphase and telophase, anillin localizes to the cortex. By preventing the cortical accumulation of anillin, astral microtubules could ensure that the contractile properties of the cell are different at the equatorial cortex versus the cell poles.

Astral and central spindle microtubules independently regulate the localization of contractile proteins

Our data suggest that astral microtubules prevent the accumulation of contractile proteins, or promote their removal. Overextending microtubules delays the cortical recruitment of

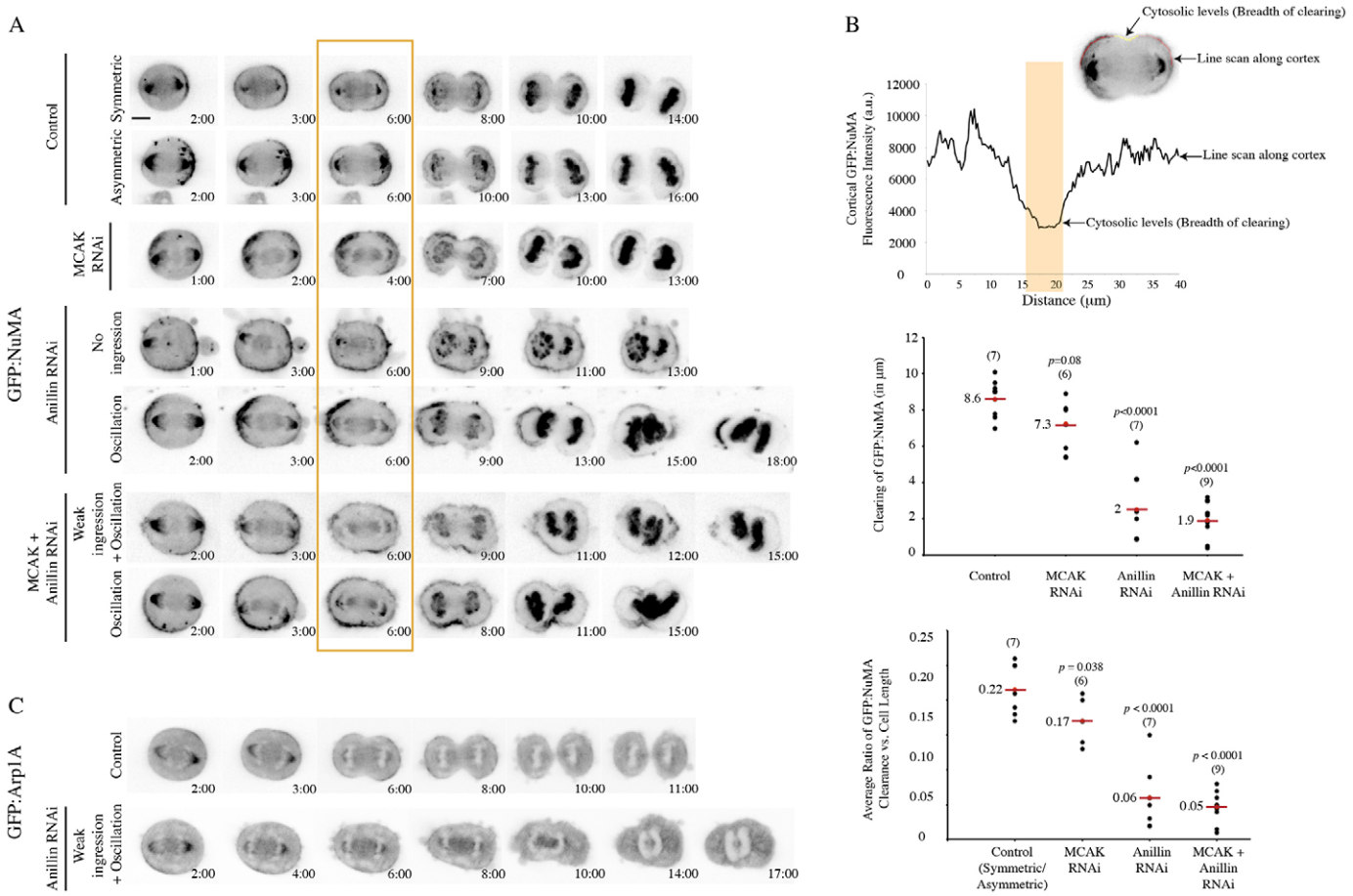

Fig. 5. Anillin regulates the localization of polar cortical proteins. (A) Images of live HeLa cells stably expressing GFP–NuMA treated with MCAK RNAi, anillin RNAi or both from anaphase onset, along with controls. The box shows the time-point used to measure NuMA clearance. Scale bar: 10 μm. (B) Upper panel, the graph shows a cortical line scan, and the pixels that correspond to cytosolic levels are highlighted by the shaded orange box. Middle panel, the graph shows the breadth of GFP–NuMA clearance for the different treatments (in μm). Lower panel, graph shows the average ratio of cleared GFP–NuMA to cell length as indicated. For the middle and lower panels, the mean is indicated by the red line; *P*-values were calculated by using Student's *t*-test; *n* values are indicated in brackets. (C) Images of live HeLa cells stably expressing GFP–Arp1A treated with anillin RNAi from anaphase onset, along with controls.

Journal of Cell Science (2014) 127, 3699–3710 doi:10.1242/jcs.147504

anillin (and RhoA) in early anaphase, and continues to restrict their localization through ingression (Fig. 1). Consistent with a model for 'removal' during telophase, we observed a correlation between the cortical localization of anillin and the boundary of astral microtubules. In particular, dots of anillin were visible on astral microtubules, some of which extend from the cortex (Fig. 2B).

The central spindle also regulates the localization of contractile proteins. In late anaphase, the directed activation of RhoA in the equatorial plane likely ensures the equatorial enrichment of contractile proteins. In MKLP1-depleted cells, Cyk-4–Ect2 complexes might ectopically activate RhoA (Fig. 1; Yüce et al., 2005). In telophase, the continued activation of RhoA in the equatorial plane keeps contractile proteins restricted to a discrete zone, permitting them to form a coalesced ring. In the absence of a central spindle, the polar astral microtubules prevent the polar accumulation of contractile proteins, but are not sufficient to sequester them to a tight zone at the equatorial cortex.

Anillin is part of the astral pathway

Anillin was previously shown to function redundantly with MKLP1, which is required for central spindle assembly (Mishima et al., 2002; Piekny and Glotzer, 2008). In HeLa cells or *C. elegans* embryos depleted of MKLP1 or anillin, furrows often form and ingress, but co-depleted cells cannot form furrows (supplementary material Fig. S4; Piekny and Glotzer, 2008; Tse et al., 2011; Werner et al., 2007). Furthermore, *C. elegans* embryos with mutations that alter the size and position of the mitotic spindle form a second 'astral' furrow that is anillin dependent (Tse et al., 2011; Werner et al., 2007). These data suggest that anillin is part of the astral pathway in both *C. elegans* and human cells. Our studies in live HeLa cells show that anillin responds to astral microtubules *in vivo*. When astral microtubules came close to the cortex, anillin cleared from these regions and blebs formed (Fig. 2D). Removal of cortical anillin could alter the organization of actin and myosin, causing changes in cortical properties. Chromatin could also mediate changes in cortical anillin localization (Kiyomitsu and Cheeseman, 2013), but the mechanism that promotes anillin removal might still involve microtubules. In the absence of microtubules (e.g. in nocodazole-treated cells), other cortical regulators, such as MP-GAP, could modulate anillin localization (Zanin et al., 2013).

RhoA might compete with microtubules for anillin binding (Fig. 3). The localization of anillin to microtubules is enriched after stabilizing microtubules with taxol or treating cells with MCAK RNAi to increase microtubule length (Fig. 3A,B). The localization of anillin to microtubules is also enhanced in C3-treated or Ect2-depleted cells, which have low levels of active RhoA (Fig. 3C). The microtubule-binding region of anillin maps to the C-terminus and might be conserved across metazoans (Fig. 3D,E). Microtubule-binding sites in other proteins appear to be helical and contain basic residues (e.g. Solinet et al., 2013). Interestingly, multiple anillin homologs have a region with stretches of basic amino acids (pI>10), which is reminiscent of the microtubule-binding region in moesin (Solinet et al., 2013). In human anillin, some of these residues were previously shown to mediate RhoA binding, and we found that they are also required for microtubule binding (Fig. 3D,E). Therefore, the association of anillin with microtubules could help to sequester the protein away from the cortex or promote its removal when active RhoA levels are low during mitosis, which could prevent premature furrowing prior to the segregation of sister chromatids.

In support of a sequestration mechanism for astral microtubules, their selective depolymerization caused an increase in the cortical levels of anillin, particularly during early mitosis (Fig. 2A). RhoA can be activated by microtubule depolymerization through the release of its activator GEF-H1 (Chang et al., 2008), which could prematurely activate RhoA and recruit anillin. However, it is not known whether this also occurs in dividing cells, where GEF-H1 is controlled by mitotic kinases (Birkenfeld et al., 2007). Furthermore, anillin stabilizes the cortical localization of RhoA (Frenette et al., 2012; Piekny and Glotzer, 2008) and a second, not mutually exclusive, hypothesis is that astral microtubules stabilize the cortical localization of RhoA through anillin. Combining nocodazole treatment with MKLP1 depletion caused anillin localization to expand to the polar cortex in half of the cells (supplementary material Fig. S3B). The equatorial localization of anillin in the other half of the cells could be due to the persistence of either central spindle or astral microtubules. Alternatively, chromatin and associated Ran–GTP could negatively regulate anillin localization at the polar cortex and influence the formation of polar blebs to stabilize the division plane (Kiyomitsu and Cheeseman, 2013; Sedzinski et al., 2011). In addition, MP-GAP could dampen cortical RhoA activity around the entire cortex, which is overcome by the upregulation of RhoGEF activity in the equatorial region of the cell (Zanin et al., 2013).

Anillin models the cortex through astral microtubules

If anillin is a component of the astral pathway that regulates the localization of contractile proteins, then removing anillin should alter how cortical proteins respond to astral microtubules. Indeed, we found that the breadth of active myosin localization decreased after MCAK depletion, but increased after co-depletion of anillin and MCAK (Fig. 4). Although active myosin localized around the entire cortex in some of the anillin-depleted cells, it was cleared from the poles in the MCAK and anillin co-depleted cells (Fig. 4). This supports the idea that multiple mechanisms regulate the localization of myosin. Anillin could be important for fine-tuning the localization of cortical proteins through astral microtubules near the equatorial cortex. Interestingly, anillin also affected the localization of NuMA and Arp1A, components of the microtubule-tethering complex and dynein–dynactin, respectively, which regulate mitotic spindle position and localize to the polar cortex (Fig. 5). For example, NuMA localized around the entire cortex both in anillin-depleted cells and in cells co-depleted of MCAK and anillin (Fig. 5A,B). Therefore, anillin is required not only for regulating the localization of equatorial proteins, but also for polar proteins. Interestingly, this data also reveals that NuMA localization is independent of myosin, and it is not clear how the mislocalization of NuMA (and Arp1A) in anillin-depleted cells relates to spindle position and the role of chromatin in clearing contractile proteins from the cell poles.

MATERIALS AND METHODS

Cell culture, transfection and drug treatments

HeLa cells were maintained in DMEM high-glucose medium supplemented with 10% FBS, 2 mM L-glutamine, 100 U penicillin and 0.1 mg/ml streptomycin as described previously (Yüce et al., 2005). Cells plated in antibiotic-free medium were transfected with siRNAs using Oligofectamine (Life Technologies) or with DNA using Lipofectamine 2000 (Life Technologies; except 4–5-fold less Lipofectamine 2000 was used than recommended by the manufacturer). Cells were transfected for 30–32 hours with MCAK, MKLP1 or anillin siRNAs as described

previously (Piekny and Glotzer, 2008; Rankin and Wordeman, 2010; Yüce et al., 2005).

The following drugs were used; nocodazole (Sigma-Aldrich) in DMSO at 30 ng/ml for 10 minutes, 10 µM taxol (Bioshop) in DMSO, 2 µM S-trityl-L-cysteine (STC; Sigma-Aldrich), 22.5 µM purvalanol A (Sigma-Aldrich) for 30 minutes (Hu et al., 2008; Shannon et al., 2005; Yüce et al., 2005) and 1 µg/ml C3 (Cytoskeleton) for 90 minutes.

GFP–MLC (active; T18E S19E) was made by QuikChange mutagenesis of mouse nonmuscle myosin light chain cDNA (gift from Michael Glotzer, University of Chicago, IL) cloned into pEGFP-C1 (BD Biosciences). A GFP–MLC (active) cell line was made by selecting positive clones after treatment with 400 µg/ml G418 (neomycin; Life Technologies) and expanding them using 200 µg/ml G418. A stable mCherry–tubulin cell line was made similarly using G418 selection. A stable line expressing GFP–NuMA (DNA generously provided by Iain Cheeseman) was generated using G418 selection. A stable line expressing anillin–GFP was generously provided by Ina Poser. A stable line expressing GFP–Arp1A was generously provided by Iain Cheeseman. The EB1-2EGFP construct was generously provided by Torsten Wittmann (University of California, San Francisco, CA). Constructs for MBP–anillin (608–1087), MBP–anillin (100–460), GFP–anillin (608–1087) and GFP–anillin (608–1087; DFEINIE – AFAINIA) were as described previously (Piekny and Glotzer, 2008).

Co-sedimentation assays

Purified protein was made from *E. coli* BL21 cells transformed with MBP–anillin (608–1087) or MBP–anillin (100–460) as described previously (Piekny and Glotzer, 2008). Bacteria were resuspended in lysis buffer [2.5 mM $MgCl_2$, 50 mM Tris, 150 mM NaCl pH 7.5, 0.5% Triton X-100, 1 mM dithiothreitol (DTT), 1 mM phenylmethanesulfonyl fluoride (PMSF) and 1× protease inhibitors; Roche], incubated with 1 µg/ml lysozyme on ice for 30 minutes, then sonicated three times. Extracts were incubated with amylose resin (New England Biolabs) for 5 hours at 4℃ with rotation. After washing, protein was stored as a 50% slurry at 4℃ and eluted in equivalent volumes of 100 mM maltose on ice for 2 hours. Protein concentration was determined before use.

Microtubules were prepared from lyophilized microtubules (Cytoskeleton) as per the manufacturer's instructions in resuspension buffer (15 mM PIPES, 1 mM $MgCl_2$, 20 µM taxol; Bioshop) at room temperature for 10–15 minutes with gentle mixing. Aliquots of 45.5 µM were flash frozen and stored at −80℃, then thawed in a circulating water bath and diluted with resuspension buffer to 9.1 µM.

Purified anillin proteins were pre-spun by centrifugation at 279,000 ***g*** for 25 minutes at room temperature. Co-sedimentation reactions were prepared in 200-µl polycarbonate tubes (Beckman Coulter) with varying concentrations of microtubules, 1 µM of purified anillin, 150 mM NaCl and BRB80 buffer (80 mM PIPES pH 6.8, 1 mM EGTA, 1 mM $MgCl_2$) containing 1 mM DTT and 10 µM taxol. The reactions were kept at room temperature for 30 minutes, then centrifuged at 279,000 ***g*** for 25 minutes. The supernatants were collected, and pellets were washed and re-suspended in BRB80. Sample buffer was added to supernatants and resuspended pellets, which were then run by SDS-PAGE and stained with Coomassie Blue. Scanned gels were analyzed in ImageJ to measure the concentration of proteins by using line plots, and pixel intensities were imported into Excel (Microsoft). After correcting for background, the average intensity was determined. The average amounts of bound anillin (*y*-axis) were plotted against microtubule concentration (*x*-axis) using GraFit version 7.0.3. The K_D and binding capacity were determined using non-linear regression ($n=3$ assays).

Westerns, fixation, immunofluorescence and live imaging

Westerns were performed after transferring SDS-PAGE gels run with 20 µg of cell lysates from cells treated with MKLP1 RNAi, MCAK RNAi, anillin RNAi or combinations thereof. Primary antibodies against MCAK (mouse; Abnova) and MKLP1 (rabbit; Santa Cruz) were used at 1:500 dilutions, and antibody against anillin (rabbit; Piekny and Glotzer, 2008) was used at 1:1000. Secondary antibodies (Alexa-Fluor-488-conjugated anti-rabbit-IgG and Alexa-Fluor-546-conjugated anti-mouse-IgG; Life Technologies) were used at 1:2500, and blots were detected using a Phosphorimager with 488 nm and 561 nm lasers (Typhoon, GE Healthcare).

Cells were fixed in 100% cold methanol or 10% cold trichloroacetic acid (TCA) as described previously (Yüce et al., 2005). The following primary antisera were used for immunofluorescence; 1:50 mouse anti-MCAK (Abnova), 1:50 rabbit anti-MKLP1 (Santa Cruz), 1:50 mouse anti-RhoA (Santa Cruz), 1:50 mouse anti-Plk1 (Santa Cruz), 1:200 rabbit anti-anillin (Piekny and Glotzer, 2008) and 1:200 mouse anti-tubulin (DM1A, Sigma-Aldrich). DNA was visualized with 1:1000 1 mg/ml DAPI (Sigma-Aldrich). To stain for both tubulin and Plk1, 1:50 goat anti-mouse-IgG antibodies (Jackson Immunoresearch) were added after incubating cells with Plk1, followed by 1:250 Alexa-Fluor-488-conjugated donkey anti-goat-IgG antisera (Jackson Immunoresearch). The following secondary antisera were used at dilutions of 1:250–1:500; Alexa-Fluor-488-conjugated anti-mouse-IgG (Life Technologies), Alexa-Fluor-568-conjugated anti-rabbit-IgG (Life Technologies), Alexa-Fluor-568-conjugated anti-mouse-IgG (Life Technologies) and Alexa-Fluor-488-conjugated anti-rabbit-IgG (Life Technologies). Images were captured on a Leica DMI6000B microscope with the 40×/1.25 NA (supplementary material Fig. S2) or 63×/1.4 NA objectives and the OrcaR2 (Hamamatsu) camera at exposure settings based on control slides using Volocity acquisition software (PerkinElmer). Images were acquired as 0.5-µm *Z*-stacks using the Piezo Z stage (Mad City Labs) and converted to TIFFs for further analyses. Images were converted to 8-bit to make figures in Adobe Photoshop and Illustrator.

Confocal images were collected using the Fluoview FV10i confocal laser scanning microscope (Olympus) with the 60×/1.35 NA objective, with an additional 8× magnification for a total magnification of 480×, using a pinhole size >50. *Z*-sections of 0.3 µm were collected per cell, and images were exported as TIFFs and converted to 8-bit images to make figures in Adobe Photoshop and Illustrator.

Live imaging was performed using IBIDI high glass bottom µ-Dish, 35 mm, either on a Leica DMI6000B microscope with the OrcaR2 (Hamamatsu) camera using Volocity (PerkinElmer) acquisition software using the 40×/1.25 NA objective and collecting multiple *Z*-stacks (0.5-µm step size, using the Piezo Z stage) every 5–15 seconds, or using the 100×/1.45 NA objective on an inverted Nikon Eclipse Ti microscope with the LiveScan Swept Field confocal microscope (Nikon), Piezo Z stage Nano-Z100-N (Mad City Labs) and the CoolSNAP HQ2 camera (Photometrics) or iXon 897 EMCCD camera (Andor) with Elements 4.0 acquisition software at 0.5-µm step sizes using a slit size of 70 µm. All images collected from the 488 channel co-imaged with 568 were spectrally unmixed using the NIS Elements Channel Unmixing software (Nikon). Cells were maintained at 37℃ under 5% CO_2 during imaging. Images were exported as TIFFs and converted into 8-bit images to make figures in Adobe Photoshop and Illustrator.

Quantifications

Measurements were performed on maximum intensity *Z*-stack projections of raw data (16-bit) in ImageJ, after background correction. External *Z*-planes were not included when measuring intensity. Mitotic cells were staged according to their shape and DNA compaction, and only cells of the same length (±2 pixels) were used for comparison (lengths were normalized by aligning cortices). To determine the ratio of anillin at the equatorial cortex, the combined total pixel intensity from a region of interest drawn around both equatorial cortices was divided by the total pixel intensity from a region drawn around the entire cell. To determine the average ratio of breadth of anillin at the equatorial region to cell length, the number of pixels with enriched anillin at the equatorial cortex was divided by the total line scan length for each cortex. To measure the breadth of GFP–MLC (active) localization, line scans were drawn along each cortex and the number of pixels with values above half the maximal value were used to calculate the breadth for each half. Ratios were calculated by dividing the breadth by the length of the cortex, which were averaged to give one value per cell. To measure the clearance of GFP–NuMA, line scans were drawn along each cortex. A second line was drawn in the cytosol, and these values were averaged to give cytosolic

intensity. The number of pixels from the cortical line scan that fell at or below this value represented the clearance of NuMA, while the total number of pixels represented cortex length. Ratios were calculated for each half of the cell, then combined to give an average value per cell. Data was imported into Excel (Microscoft), where sample size, mean, standard deviations and/or standard error of the mean were calculated and graphs were generated.

Acknowledgements
We thank the Centre for Microscopy at Concordia for imaging expertise. Thanks to Madhav Soowamber and Michelle Ricci (both of Concordia University, Montreal, Canada) for their technical contributions. We thank Karen Oegema (University of California, San Diego, La Jolla, CA) and Esther Zanin (Ludwig-Maximilians University, Munich, Germany) for intellectual contributions. We thank Iain Cheeseman (Whitehead Institute, Cambridge, MA), Esther Zanin, Torsten Wittmann (University of California, San Francisco, CA) and Ina Poser (Max Planck Institute of Molecular Cell Biology and Genetics, Dresden, Germany) for reagents.

Competing interests
The authors declare no competing interests.

Author contributions
All authors provided intellectual contribution. C.O.T. contributed to Figs 2–5 and supplementary material Fig. S4; M.J.G. contributed to Figs 2–3 and supplementary material Figs S1,2; H.H.B. contributed to Figs 1–3 and supplementary material Fig. S3; D.B. contributed to Fig. 3; and A.P. contributed to Figs 1–5 and supplementary material Figs S2–4, and wrote the manuscript.

Funding
This work was supported by Fonds de recherche du Québec [grant number 131473 to A.P.]; and the Canadian Institutes of Health Research [grant number 93630 to A.P.].

Supplementary material
Supplementary material available online at
http://jcs.biologists.org/lookup/suppl/doi:10.1242/jcs.147504/-/DC1

References
Bement, W. M., Benink, H. A. and von Dassow, G. (2005). A microtubule-dependent zone of active RhoA during cleavage plane specification. *J. Cell Biol.* **170**, 91-101.
Birkenfeld, J., Nalbant, P., Bohl, B. P., Pertz, O., Hahn, K. M. and Bokoch, G. M. (2007). GEF-H1 modulates localized RhoA activation during cytokinesis under the control of mitotic kinases. *Dev. Cell* **12**, 699-712.
Bringmann, H. and Hyman, A. A. (2005). A cytokinesis furrow is positioned by two consecutive signals. *Nature* **436**, 731-734.
Bringmann, H., Cowan, C. R., Kong, J. and Hyman, A. A. (2007). LET-99, GOA-1/GPA-16, and GPR-1/2 are required for aster-positioned cytokinesis. *Curr. Biol.* **17**, 185-191.
Canman, J. C., Hoffman, D. B. and Salmon, E. D. (2000). The role of pre- and post-anaphase microtubules in the cytokinesis phase of the cell cycle. *Curr. Biol.* **10**, 611-614.
Canman, J. C., Cameron, L. A., Maddox, P. S., Straight, A., Tirnauer, J. S., Mitchison, T. J., Fang, G., Kapoor, T. M. and Salmon, E. D. (2003). Determining the position of the cell division plane. *Nature* **424**, 1074-1078.
Carmena, M., Wheelock, M., Funabiki, H. and Earnshaw, W. C. (2012). The chromosomal passenger complex (CPC): from easy rider to the godfather of mitosis. *Nat. Rev. Mol. Cell Biol.* **13**, 789-803.
Chang, Y. C., Nalbant, P., Birkenfeld, J., Chang, Z. F. and Bokoch, G. M. (2008). GEF-H1 couples nocodazole-induced microtubule disassembly to cell contractility via RhoA. *Mol. Biol. Cell* **19**, 2147-2153.
D'Avino, P. P., Takeda, T., Capalbo, L., Zhang, W., Lilley, K. S., Laue, E. D. and Glover, D. M. (2008). Interaction between Anillin and RacGAP50C connects the actomyosin contractile ring with spindle microtubules at the cell division site. *J. Cell Sci.* **121**, 1151-1158.
Dechant, R. and Glotzer, M. (2003). Centrosome separation and central spindle assembly act in redundant pathways that regulate microtubule density and trigger cleavage furrow formation. *Dev. Cell* **4**, 333-344.
Foe, V. E. and von Dassow, G. (2008). Stable and dynamic microtubules coordinately shape the myosin activation zone during cytokinetic furrow formation. *J. Cell Biol.* **183**, 457-470.
Frenette, P., Haines, E., Loloyan, M., Kinal, M., Pakarian, P. and Piekny, A. (2012). An anillin-Ect2 complex stabilizes central spindle microtubules at the cortex during cytokinesis. *PLoS ONE* **7**, e34888.
Glotzer, M. (2009). The 3Ms of central spindle assembly: microtubules, motors and MAPs. *Nat. Rev. Mol. Cell Biol.* **10**, 9-20.
Green, R. A., Paluch, E. and Oegema, K. (2012). Cytokinesis in animal cells. *Annu. Rev. Cell Dev. Biol.* **28**, 29-58.
Gregory, S. L., Ebrahimi, S., Milverton, J., Jones, W. M., Bejsovec, A. and Saint, R. (2008). Cell division requires a direct link between microtubule-bound RacGAP and Anillin in the contractile ring. *Curr. Biol.* **18**, 25-29.
Hu, C. K., Coughlin, M., Field, C. M. and Mitchison, T. J. (2008). Cell polarization during monopolar cytokinesis. *J. Cell Biol.* **181**, 195-202.
Kiyomitsu, T. and Cheeseman, I. M. (2012). Chromosome- and spindle-pole-derived signals generate an intrinsic code for spindle position and orientation. *Nat. Cell Biol.* **14**, 311-317.
Kiyomitsu, T. and Cheeseman, I. M. (2013). Cortical dynein and asymmetric membrane elongation coordinately position the spindle in anaphase. *Cell* **154**, 391-402.
Krendel, M., Zenke, F. T. and Bokoch, G. M. (2002). Nucleotide exchange factor GEF-H1 mediates cross-talk between microtubules and the actin cytoskeleton. *Nat. Cell Biol.* **4**, 294-301.
Lekomtsev, S., Su, K. C., Pye, V. E., Blight, K., Sundaramoorthy, S., Takaki, T., Collinson, L. M., Cherepanov, P., Divecha, N. and Petronczki, M. (2012). Centralspindlin links the mitotic spindle to the plasma membrane during cytokinesis. *Nature* **492**, 276-279.
Lewellyn, L., Dumont, J., Desai, A. and Oegema, K. (2010). Analyzing the effects of delaying aster separation on furrow formation during cytokinesis in the Caenorhabditis elegans embryo. *Mol. Biol. Cell* **21**, 50-62.
Mishima, M., Kaitna, S. and Glotzer, M. (2002). Central spindle assembly and cytokinesis require a kinesin-like protein/RhoGAP complex with microtubule bundling activity. *Dev. Cell* **2**, 41-54.
Murthy, K. and Wadsworth, P. (2008). Dual role for microtubules in regulating cortical contractility during cytokinesis. *J. Cell Sci.* **121**, 2350-2359.
Oegema, K., Savoian, M. S., Mitchison, T. J. and Field, C. M. (2000). Functional analysis of a human homologue of the Drosophila actin binding protein anillin suggests a role in cytokinesis. *J. Cell Biol.* **150**, 539-552.
Petronczki, M., Glotzer, M., Kraut, N. and Peters, J. M. (2007). Polo-like kinase 1 triggers the initiation of cytokinesis in human cells by promoting recruitment of the RhoGEF Ect2 to the central spindle. *Dev. Cell* **12**, 713-725.
Piekny, A. J. and Glotzer, M. (2008). Anillin is a scaffold protein that links RhoA, actin, and myosin during cytokinesis. *Curr. Biol.* **18**, 30-36.
Piekny, A. J. and Maddox, A. S. (2010). The myriad roles of Anillin during cytokinesis. *Semin. Cell Dev. Biol.* **21**, 881-891.
Piekny, A., Werner, M. and Glotzer, M. (2005). Cytokinesis: welcome to the Rho zone. *Trends Cell Biol.* **15**, 651-658.
Rankin, K. E. and Wordeman, L. (2010). Long astral microtubules uncouple mitotic spindles from the cytokinetic furrow. *J. Cell Biol.* **190**, 35-43.
Saito, S., Tatsumoto, T., Lorenzi, M. V., Chedid, M., Kapoor, V., Sakata, H., Rubin, J. and Miki, T. (2003). Rho exchange factor ECT2 is induced by growth factors and regulates cytokinesis through the N-terminal cell cycle regulator-related domains. *J. Cell. Biochem.* **90**, 819-836.
Sedzinski, J., Biro, M., Oswald, A., Tinevez, J. Y., Salbreux, G. and Paluch, E. (2011). Polar actomyosin contractility destabilizes the position of the cytokinetic furrow. *Nature* **476**, 462-466.
Shannon, K. B., Canman, J. C., Ben Moree, C., Tirnauer, J. S. and Salmon, E. D. (2005). Taxol-stabilized microtubules can position the cytokinetic furrow in mammalian cells. *Mol. Biol. Cell* **16**, 4423-4436.
Solinet, S., Mahmud, K., Stewman, S. F., Ben El Kadhi, K., Decelle, B., Talje, L., Ma, A., Kwok, B. H. and Carreno, S. (2013). The actin-binding ERM protein Moesin binds to and stabilizes microtubules at the cell cortex. *J. Cell Biol.* **202**, 251-260.
Somers, W. G. and Saint, R. (2003). A RhoGEF and Rho family GTPase-activating protein complex links the contractile ring to cortical microtubules at the onset of cytokinesis. *Dev. Cell* **4**, 29-39.
Su, K. C., Takaki, T. and Petronczki, M. (2011). Targeting of the RhoGEF Ect2 to the equatorial membrane controls cleavage furrow formation during cytokinesis. *Dev. Cell* **21**, 1104-1115.
Tse, Y. C., Piekny, A. and Glotzer, M. (2011). Anillin promotes astral microtubule-directed cortical myosin polarization. *Mol. Biol. Cell* **22**, 3165-3175.
Verbrugghe, K. J. and White, J. G. (2004). SPD-1 is required for the formation of the spindle midzone but is not essential for the completion of cytokinesis in C. elegans embryos. *Curr. Biol.* **14**, 1755-1760.
von Dassow, G., Verbrugghe, K. J., Miller, A. L., Sider, J. R. and Bement, W. M. (2009). Action at a distance during cytokinesis. *J. Cell Biol.* **187**, 831-845.
Werner, M., Munro, E. and Glotzer, M. (2007). Astral signals spatially bias cortical myosin recruitment to break symmetry and promote cytokinesis. *Curr. Biol.* **17**, 1286-1297.
Wolfe, B. A., Takaki, T., Petronczki, M. and Glotzer, M. (2009). Polo-like kinase 1 directs assembly of the HsCyk-4 RhoGAP/Ect2 RhoGEF complex to initiate cleavage furrow formation. *PLoS Biol.* **7**, e1000110.
Yüce, O., Piekny, A. and Glotzer, M. (2005). An ECT2-centralspindlin complex regulates the localization and function of RhoA. *J. Cell Biol.* **170**, 571-582.
Zanin, E., Desai, A., Poser, I., Toyoda, Y., Andree, C., Moebius, C., Bickle, M., Conradt, B., Piekny, A. and Oegema, K. (2013). A conserved RhoGAP limits M phase contractility and coordinates with microtubule asters to confine RhoA during cytokinesis. *Dev. Cell* **26**, 496-510.
Zhao, W. M. and Fang, G. (2005a). Anillin is a substrate of anaphase-promoting complex/cyclosome (APC/C) that controls spatial contractility of myosin during late cytokinesis. *J. Biol. Chem.* **280**, 33516-33524.
Zhao, W. M. and Fang, G. (2005b). MgcRacGAP controls the assembly of the contractile ring and the initiation of cytokinesis. *Proc. Natl. Acad. Sci. USA* **102**, 13158-13163.